Defining long range order in NMR structure determination from the dependence of heteronuclear relaxation times on rotational diffusion anisotropy

Nico Tjandra[1,2], Daniel S. Garrett[1], Angela M. Gronenborn[1], Ad Bax[1] and G. Marius Clore[1]

Structure determination by NMR presently relies on short range restraints between atoms in close spatial proximity, principally in the form of short (< 5 Å) interproton distances. In the case of modular or multidomain proteins and linear nucleic acids, the density of short interproton distance contacts between structural elements far apart in the sequence may be insufficient to define their relative orientations. In this paper we show how the dependence of heteronuclear longitudinal and transverse relaxation times on the rotational diffusion anisotropy of non-spherical molecules can be readily used to directly provide restraints for simulated annealing structure refinement that characterize long range order *a priori*. The method is demonstrated using the N-terminal domain of Enzyme I, a protein of 259 residues comprising two distinct domains with a diffusion anisotropy ($D_{\|}/D_{\perp}$) of ~2.

Current methods of macromolecular structure determination by NMR rely exclusively on restraints whose information is entirely local and restricted to atoms close in space, namely short (<5 Å) interproton distances and torsion angles[1,2]. The success of these methods is due to the fact that short interproton distances between units far apart in a linear array are conformationally highly restrictive. However, there are numerous cases where restraints that define long range order can supply invaluable structural information. In particular, they permit the relative positioning of structural elements that do not have many short interproton distance contacts between them. Examples of such situations include modular and multidomain proteins and linear nucleic acids[2,3]. Here we show that the dependence of ^{15}N relaxation on rotational diffusion anisotropy can directly provide structural restraints for simulated annealing refinement that determine the orientation of N–H vectors relative to an external axis and hence characterize long range order.

Theory

Heteronuclear relaxation has long been used to provide information on internal dynamics[4–10]. The ^{15}N transverse relaxation time T_2 is a function of frequency-dependent and -independent spectral density terms, while the ^{15}N longitudinal relaxation time T_1 is only a function of the frequency-dependent terms[11]. For axially symmetric rotational diffusion (that is, $D_{zz} \neq D_{xx} = D_{yy}$ where D_{zz}, D_{xx}, D_{yy} are the diagonal elements of the diffusion tensor) characterized by diffusion tensor constants parallel ($D_{\|} = D_{zz}$) and perpendicular ($D_{\perp} = [D_{xx} + D_{yy}]/2$) to the unique axis of the diffusion tensor, the spectral density $J(\omega)$, in the limit of very fast, axially symmetric internal motions, is given by[5,12]

$$J(\omega) = S^2\Sigma_{k=1,2,3}A_k[\tau_k/(1+\omega^2\tau_k^2)] \quad (1)$$

where ω is the angular resonance frequency, and S the generalized order parameter for rapid internal motion; τ_1, τ_2 and τ_3 are time constants given by $(6D_{\perp})^{-1}$, $(D_{\|} + 5D_{\perp})^{-1}$ and $(4D_{\|} + 2D_{\perp})^{-1}$; and the terms A_1, A_2 and A_3 are given by $(1.5\cos^2\theta - 0.5)^2$, $3\sin^2\theta\cos^2\theta$ and $0.75\sin^4\theta$, where θ is the angle between the time-averaged N–H bond vector orientation in the molecular frame and the unique axis of the diffusion tensor.

In the absence of large amplitude internal motions and conformational exchange line broadening, the ^{15}N T_1/T_2 ratio for a protein with an axially symmetric diffusion tensor depends only on three variables: the angle θ (arising from the A_k terms in Eq. 1), and the diffusion tensor constants $D_{\|}$ and $D_{\perp}$[5,12–14]. As described below, $D_{\|}$ and $D_{\perp}$ are readily extracted from the ensemble of ^{15}N T_1 and T_2 relaxation times. Thus, the individual T_1/T_2 ratios provide a direct measure of the angle θ between the N–H bond vector and the unique axis of the diffusion tensor. As this orientation is not known *a priori*, we allow it to float by making use of an external, initially arbitrarily positioned axis, defined by a single C–C bond, positioned 50 Å away from the structure. The geometric content of the T_1/T_2 ratios can then be incorporated into the simulated annealing protocol[15] used for structure determination by minimizing the quadratic harmonic potential term E_{anis}

$$E_{anis} = k_{anis}[(T_1/T_2)_{calc} - (T_1/T_2)_{obs}]^2 \quad (2)$$

where k_{anis} is a 'force constant', and $(T_1/T_2)_{obs}$ and $(T_1/T_2)_{calc}$ are the observed and calculated values of T_1/T_2 respectively. At

[1]Laboratory of Chemical Physics, Building 5, National Institutes of Diabetes and Digestive and Kidney Diseases, National Institutes of Health, Bethesda, Maryland 20892-0520, USA. [2]Laboratory of Biophysical Chemistry, Building 3, National Heart, Lung and Blood Institute, National Institutes of Health, Bethesda, MD 20892-0380, USA
The first two authors contributed equally to the work.

Correspondence should be addressed to G.M.C. *email: clore@vger.niddk.nih.gov*

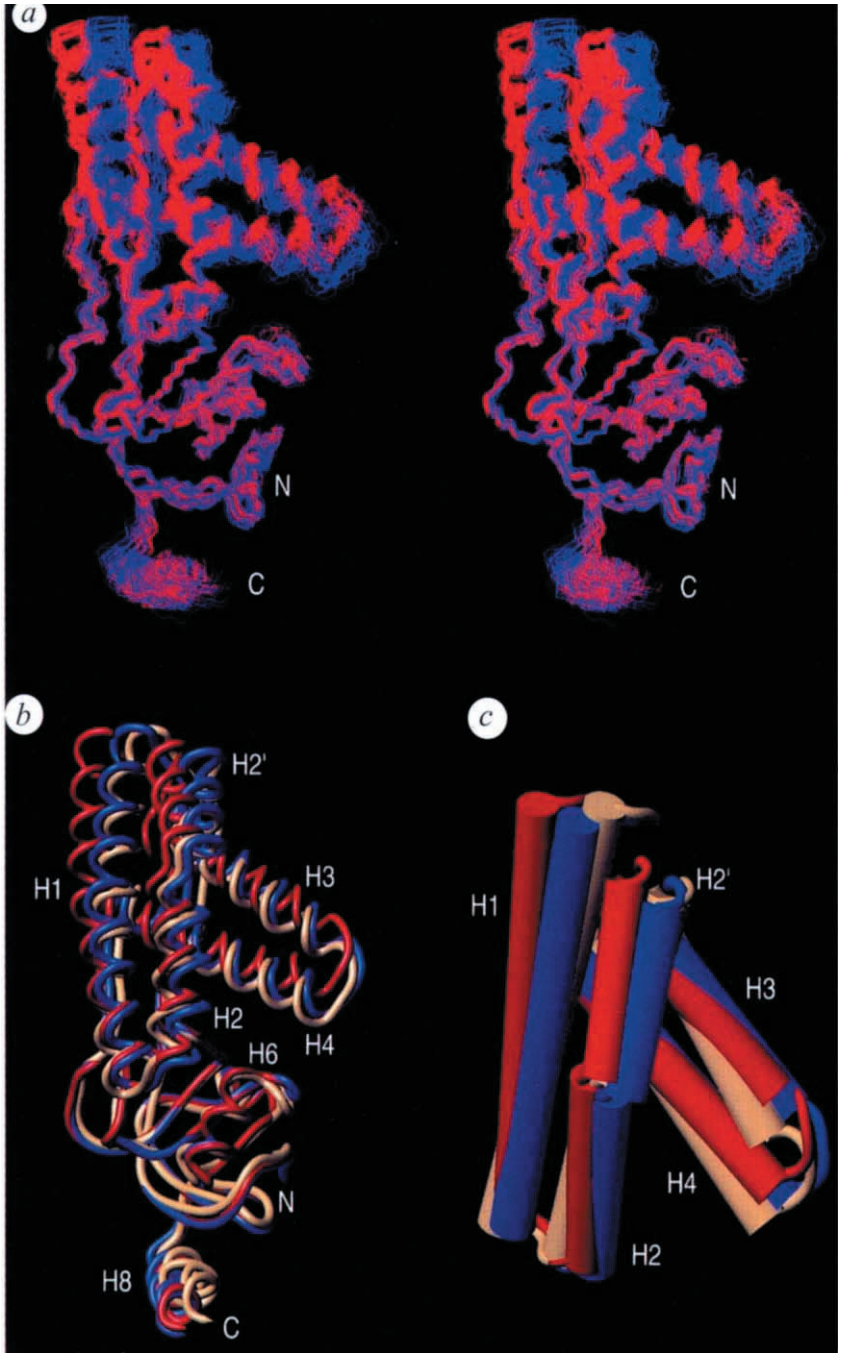

Fig. 1 ***a***, Best-fit superposition of the backbone (N, Cα, C) atoms of the ensemble of simulated annealing structures (30 each) of EIN calculated with (red) and without (blue) ^{15}N T_1/T_2 refinement, best-fitted to the α/β domain (residues 2–20 and 148–230). ***b*** and ***c***, Views showing superpositions, best-fitted to the α/β domain, of the restrained regularized mean structures derived from the ensembles calculated with (red) and without (blue) ^{15}N T_1/T_2 refinement, and of the X-ray structure (yellow). In (*b*) the backbone of residues 1–249 is displayed as a tubular representation; in (*c*) the helices of the α domain are shown as cylinders. This figure was generated with the program MOLMOL[22]. Simulated annealing calculations[15] were carried out with the program X-PLOR-31[23] modified to include terms for three-bond *J* coupling[24], secondary ^{13}C shifts[25], and heteronuclear relaxation refinement. The target function employed for simulated annealing comprised terms for covalent geometry, NOE derived interproton distance restraints, torsion angle restraints, $^3J_{HNH\alpha}$ coupling constant restraints, secondary ^{13}C shifts restraints, ^{15}N T_1/T_2 restraints, and a quartic van der Waals repulsion potential.

each step of the simulated annealing protocol, E_{anis} is evaluated by calculating the angle between the N–H vectors and the unique axis of the diffusion tensor, defined by the floating C–C bond vector. Since actual values of T_1/T_2 (with a known degree of uncertainty) are determined experimentally, a harmonic potential, rather than a square-well potential, is employed for E_{anis}. We note that under these circumstances, a harmonic potential is not only preferable on statistical grounds but, in addition, displays superior convergence properties relative to those of a square-well potential. The desired target value between observed and calculated T_1/T_2 ratios, based on the experimental uncertainty in the measured T_1/T_2 values, is achieved by empirically adjusting the value of k_{anis}.

For the method to be applicable the molecule must obviously tumble anisotropically (that is, $D_{||}/D_{\perp} > 1$). The minimum ratio of $D_{||}/D_{\perp}$ for which heteronuclear T_1/T_2 refinement will be useful depends entirely on the accuracy and uncertainties in the measured T_1/T_2 ratios. In practice, $[(T_1/T_2)_{max} - (T_1/T_2)_{min}]$ must exceed the uncertainty in the measured T_1/T_2 values by an order of magnitude. This typically means that $D_{||}/D_{\perp}$ should be greater than ~1.5.

Application to EIN

To address the utility of this approach, we have tested the method on the N-terminal domain of enzyme I (EIN) of the PTS pathway, for which X-ray[16] and NMR[17] structures have recently been deter-

Table 1 Structure statistics[1]

	<SA_{anis}>	<SA>	X-ray
R.m.s. deviations in experimental restraints			
T_1/T_2 (117)	0.94 ± 0.03	2.91 ± 0.12	2.66
Distance restraints (Å) (3048)	0.031 ± 0.001	0.026 ± 0.006	0.179
Torsion angle restraints (°) (543)	0.248 ± 0.040	0.193 ± 0.023	30.9
$^3J_{HN\alpha}$ (Hz) (163)	0.719 ± 0.021	0.611 ± 0.011	2.11
$^{13}C\alpha$ shifts (p.p.m.) (257)	1.12 ± 0.02	1.08 ± 0.02	1.31
$^{13}C\beta$ shifts (p.p.m.) (241)	0.97 ± 0.02	0.96 ± 0.01	1.10
R.m.s. deviations in covalent geometry			
bonds (Å) (4045)	0.003 ± 0.0001	0.003 ± 0.001	0.024
angles (°) (7373)	0.398 ± 0.014	0.351 ± 0.010	2.60
impropers (°) (1954)	0.423 ± 0.020	0.347 ± 0.033	3.07
PROCHECK parameters[2]			
% residues in most favourable region of Ramachandran plot	86.0 ± 1.3	85.1 ± 1.17	87.7
no. bad contacts/100 residues	6.8 ± 1.4	7.0 ± 1.45	2.0

[1]<SA_{anis}> and <SA> are the final 30 simulated annealing structures calculated with and without the incorporation of ^{15}N T_1/T_2 restraints; $\overline{SA}_{anis}$ and $\overline{SA}$ are the corresponding mean structures obtained by averaging the coordinates of the individual SA_{anis} and SA structures (residues 2–246), respectively, best-fitted to each other. $(\overline{SA}_{anis})r$ and $(\overline{SA})r$ are the restrained regularized mean structures obtained by restrained regularization of the mean structures $\overline{SA}_{anis}$ and $\overline{SA}$ respectively. The NMR structures were calculated for the complete EIN domain comprising residues 1–259. In the case of the X-ray structure only residues 2–249 are visible in the electron density map[16]. The number of terms for the various restraints is given in parentheses. The experimental NMR distance, torsion, three-bond coupling constant and ^{13}C shift restraints are taken from ref. 17. The final force constants employed for the various terms in the target function used for simulated annealing are as follows: 1,000 kcal mol^{-1} $Å^{-2}$ for bond lengths, 500 kcal mol^{-1} rad^{-2} for angles and improper torsions (which serve to maintain planarity and chirality); 4 kcal mol^{-1} $Å^{-4}$ for the quartic van der Waals repulsion term (with the hard sphere effective van der Waals radius set to 0.8 times their values used in the CHARMM PARAM19/20 parameters[29]), 30 kcal mol^{-1} $Å^{-2}$ for the experimental distance restraints (which comprise 2,818 interproton distance and 230 backbone hydrogen bonding restraints), 200 kcal mol^{-1} rad^{-2} for the torsion angle restraints, 1 kcal mol^{-1} Hz^{-2} for the three-bond coupling constant restraints, 0.5 kcal mol^{-1} p.p.m.$^{-2}$ for the carbon chemical shift restraints, and in the case of the <SA_{anis}> structures 1 kcal mol^{-1} for the T_1/T_2 ratio restraints.
[2]The program PROCHECK[30] was used to check the quality of the structures.

mined. EIN is a 259 residue, 30,000 M_r protein, comprising two domains, an α domain (residues 33–143) consisting of four helices, and an α/β domain (residues 2–20 and 148–230) consisting of three helices and six β-strands. In addition, there is a C-terminal helix (residues 233–250) which serves as a linker to the C-terminal domain of enzyme I. Of the 2818 NOEs used to determine the NMR structure of EIN, only 38 involve interdomain contacts. The molecule is axially symmetric with a ratio of 3:3:1 for the principal components of the inertia tensor, yielding a predicted diffusion anisotropy $D_{||}/D_\perp$ of ~2.1. The assumption of axially symmetric diffusion was further tested by best-fitting the observed T_1/T_2 ratios to the calculated values obtained from the X-ray and original NMR structure using both fully asymmetric and axially symmetric diffusion models[13,14]. This yielded an overall effective rotational correlation time of 13.1 ns, and no improvements in the fits were found upon inclusion of a rhombic component (i.e. the fully asymmetric model with $D_{xx} \neq D_{yy}$) which was found to have D_{xx}/D_{yy} values of 1.01–1.03.

After excluding residues with insufficiently resolved ^1H–^{15}N correlations, amides which display significant internal motions faster than the overall rotational diffusion (characterized by a $^{15}N\{-^1H\}$ NOE ≤ 0.65)[6,7,13], and amides which undergo conformational exchange (identified using the criteria of Tjandra *et al.*[14]), 117 T_1/T_2 values were available for analysis, 61 from the α/β domain and 56 from the α domain. Because of the large number of amide groups (a total of 254) and the limited spectral dispersion of EIN, 100 residues were excluded due to spectral overlap which precluded accurate T_1, T_2 and ^{15}N-$\{^1H\}$ NOE data from being obtained. Limited spectral resolution will always present a problem for proteins the size of EIN but can be readily circumvented by making use of amino acid-specific labeling to simplify the spectrum. Of the 154 residues for which reliable ^{15}N relaxation data could be obtained, only 37, all located in loops, had to be excluded because of motional considerations. Indeed, heteronuclear relaxation studies on a wide range of proteins have shown that regions of high mobility are generally confined to loops while the secondary structure elements are relatively rigid[6–10,13,14]. Consequently, the elimination of highly mobile residues does not present a limitation of the method since long range order is best defined in terms of the relative orientations of the secondary structure elements.

The r.m.s. error in the experimental T_1/T_2 ratios is 0.3, and the observed T_1/T_2 ratios span a range from ~14 to ~27. Given uncertainties of up to ±5° in the position of the NH vector relative to the peptide plane[18,19], and uncertainties of up to ±10% in the values of $D_{||}$ and $D_\perp$, the estimated target error for the T_1/T_2 ratios is 1.0. Empirically, we found that this target value was best achieved using a value of 1.0 kcal mol^{-1} for the 'force constant' k_{anis}.

Determination of DII and $D_\perp$

In order to apply Eq. (2) for structure refinement, the values of $D_{||}$ and $D_\perp$ must be determined directly from the ensemble of measured T_1/T_2 ratios without reference to a known structure. If the structure, and hence the positions of the N–H vectors, are known, the orientation of the unique axis of the diffusion tensor and the values of $D_{||}$ and $D_\perp$ can of course be obtained by non-linear optimization, best-fitting the observed T_1/T_2 ratios to the calculated values derived from the structure[13,14,20]. For a uniform distribution of N–H bond vectors in space, the probability of finding an N–H vector that makes an angle θ with the unique axis of the diffusion tensor is proportional to sinθ. Hence, θ values near 90° are statistically most probable. These are the amides that yield the lowest T_1/T_2 ratios. The probability of finding an N–H bond vector with θ ≈ 0° is low, and, consequently, the T_1/T_2 ratio for θ = 0° is not as easily extracted from the range of experimentally observed T_1/T_2 ratios. Experimentally, $(T_1/T_2)_{min}$ and an initial estimate of $(T_1/T_2)_{max}$ are obtained by taking the average of the lowest and highest T_1/T_2 ratios, respectively, such that the standard deviations in their estimates are equal to the measurement error (in this case ± 0.3). Initial estimates for $D_{||}$ and $D_\perp$ are then obtained by simultaneously best-fitting the complete equations describing $(T_1/T_2)_{min}$, $(T_1/T_2)_{max}$, and the ratio of these two terms. The experimental value of $(T_1/T_2)_{min}$ is 14.48, and the initial estimate of $(T_1/T_2)_{max}$ is 26.46, yielding starting values of 18.0×10^7 s^{-1} and 10.2×10^7 s^{-1} for $D_{||}$ and $D_\perp$ respectively. Since the initial estimate of $(T_1/T_2)_{max}$ is likely to underestimate the true value of $(T_1/T_2)_{max}$, the value of $(T_1/T_2)_{max}$ is therefore increased in a stepwise manner (in increments of 5% up to a 35% increase) yielding new values of $D_{||}$ and $D_\perp$. For each set of values, an ensemble of simulated annealing structures is calculated with the same value of the force constant k_{anis} (1.0 kcal mol^{-1}) in Eq. 2. Best agreement between the observed and calculated T_1/T_2 values

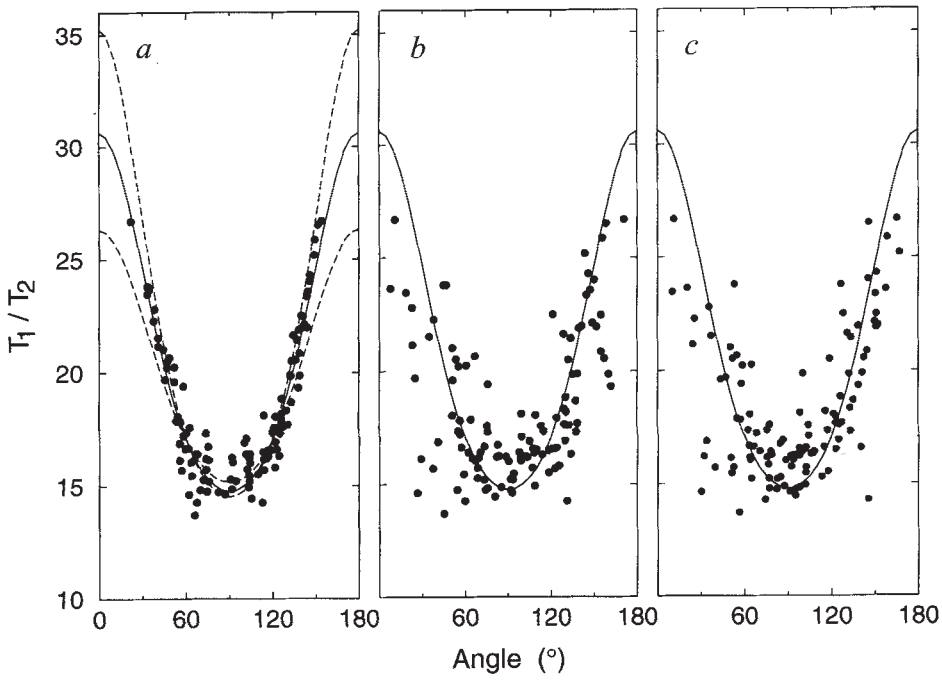

Fig. 2 Dependence of the observed ^{15}N T_1/T_2 ratios at 600 MHz on the angle θ between the NH bond vectors and the unique axis of the diffusion tensor for the restrained regularized mean structures of EIN obtained from the ensembles calculated ***a***, with and ***b***, without ^{15}N T_1/T_2 refinement, and ***c***, for the X-ray structure. The solid lines represent the theoretical dependence of T_1/T_2 versus θ for a diffusion anisotropy of 2.1 and an effective correlation time of 13.1 ns. The dashed lines in (*a*) illustrate the effects on the theoretical dependence of T_1/T_2 versus θ of increasing or decreasing the diffusion anisotropy by 15%. Note that the dependence of T_1/T_2 versus θ can be approximated to within an error of less than 0.5% by a cosine expansion of the form $T_1/T_2 = A + B\cos(2\theta) + C\cos(4\theta)$. Uniformly ^{15}N and ^{2}H labeled EIN was prepared as described by Garrett *et al.*[17]. Samples for NMR contained 1.1 mM protein in 40 mM sodium phosphate buffer pH 7.0 and 90% H_2O/10% D_2O. ^{15}N labelling was >99% and ^{2}H labelling of non-exchangeable protons was >90%. Deuteration of non-exchangeable protons narrows the ^{1}H linewidth, thereby reducing spectral overlap. All NMR spectra were collected at 40 °C on a Bruker DMX600 spectrometer operating at a ^{1}H frequency of 600 MHz and equipped with a *x,y,z* gradient triple resonance probe. ^{15}N T_1 and $T_{1\rho}$ data were collected using previously described pulse sequences[26,27] with added pulsed-field gradients for improved suppression of artifacts and of the water signal[14]. ^{15}N T_2 values were derived from the T_1 and $T_{1\rho}$ values using the equation $T_{1\rho} = (\cos^2\lambda/T_2 + \sin^2\lambda/T_1)$ where $\lambda = \tan^{-1}(\Omega_N/\gamma_N B_1)$, $\Omega_N/2\pi$ is the resonance offset, and $\gamma_N B_1/2\pi$ is the strength of the ^{15}N spin-lock field (2.5 kHz)[14]. Heating effects at even the longest ^{15}N spin-lock period were measured to be less than 0.1 °C[14]. Based on duplicate and quadruplicate experiments for T_1 and $T_{1\rho}$, respectively, the random error in the T_1/T_2 ratios is ±0.3. ^{15}N-{^{1}H} NOEs were measured using the water flip-back method[28]. Of the 254 backbone amide groups in EIN, 100 were excluded because of insufficiently resolved ^{1}H-^{15}N correlations and a further 37, all located in loops, were excluded because of significant internal motions (manifested by ^{15}N-{^{1}H} NOE values less than 0.65 or by conformational exchange on a μs to ms time scale), resulting in 117 T_1/T_2 values available for analysis.

is found for $D_{\parallel} = 19.55 \times 10^6\ s^{-1}$ and $D_{\perp} = 9.31 \times 10^6\ s^{-1}$, corresponding to a value of 13.1 ns for the effective overall rotational correlation time $\tau_{c,eff} = (2D_{\parallel} + 4D_{\perp})^{-1}$, a diffusion anisotropy $D_{\parallel}/D_{\perp}$ of 2.1, and a value of 2.24 for $(T_1/T_2)_{max}/(T_1/T_{2)min}$. This minimum is relatively shallow, and the structure is not significantly affected by using $D_{\parallel}$ and $D_{\perp}$ values that change $(T_1/T_2)_{max}$ by up to ±15%, but keep $(T_1/T_2)_{min}$ constant. Indeed, the overall backbone r.m.s. difference (residues 2–246) between structures calculated with $(T_1/T_2)_{max}/(T_1/T_{2)min} = 1.9$ and 2.5 is only 0.3 Å, which is well inside the precision of the coordinates (~0.8 Å).

Structural statistics

A summary of the structural statistics and atomic r.m.s. shifts is provided in Tables 1 and 2, respectively, and a best-fit superposition of the two ensembles of NMR structures calculated with (SA_{anis}) and without (SA) refinement against the ^{15}N T_1/T_2 ratios is shown in Fig. 1*a*. The r.m.s. difference between observed and calculated T_1/T_2 ratios for the SA and X-ray structures is 2.7–2.9. This is reduced to a value of 0.94 ± 0.03 upon ^{15}N T_1/T_2 refinement, without a detrimental impact on the agreement with the other experimental NMR restraints, the covalent geometry, the nonbonded contacts and the quality of the Ramachandran plot (Table 1). In addition, we note the excellent agreement between the unique axis of the inertia tensor calculated from the atomic coordinates and the unique axis of the diffusion tensor represented by the C–C vector employed in the simulated annealing calculations, which differ by less than 2°. The dependence of the observed T_1/T_2 ratios on the angle θ calculated from the restrained regularized mean structures derived from the $<\overline{SA}_{anis}>$ and $<\overline{SA}>$ ensembles of structures, $(SA_{anis})r$ and $(\overline{SA})r$, respectively, as well as from the X-ray structure, is shown in Fig. 2. While all three structures show a clear dependence of the T_1/T_2 ratios on the angle θ, the scatter for the $(\overline{SA})r$ structure and the X-ray structure is relatively large. The dependence of T_1/T_2 ratios on θ for the $(\overline{SA}_{anis})r$ structure, however, matches the theoretical dependence closely.

Structural consequences of refinement against T_1/T_2 ratios

Comparison of the $<SA_{anis}>$ and <SA> ensembles of structures indicates that the precision of the coordinates of the α and α/β domains individually is about the same (0.5–0.6 Å) and that the atomic r.m.s. shift between the mean coordinate positions for these two domains is small (0.3–0.4 Å). Hence, incorporation of ^{15}N T_1/T_2 restraints has very little effect on the structures of the individual domains. Moreover, the backbone r.m.s. difference between the X-ray structure and the two NMR structures for the two domains independently is approximately the same (~0.9 Å for the α domain, and ~1.2 Å for the α/β domain). The key difference between the three structures therefore lies in the relative orientations of the two domains. This is readily apparent from the superpositions shown in Fig. 1. Fig. 1*a* shows a superposition of the $<SA_{anis}>$ and <SA> ensembles of NMR structures best-fitted to the α/β domain. Fig. 1*b* and 1*c* show two views of a superposition of the corresponding regularized mean NMR structures, $(\overline{SA}_{anis})r$ and $(\overline{SA})r$, and the X-ray structure, also best-fitted to the α/β domain. The atomic r.m.s. displacements between the α domains in these best-fits are large (2–3 Å). Moreover, the α domain in the $(\overline{SA}_{anis})r$ structure is displaced slightly further from the X-ray structure than that of the $(\overline{SA})r$ structure.

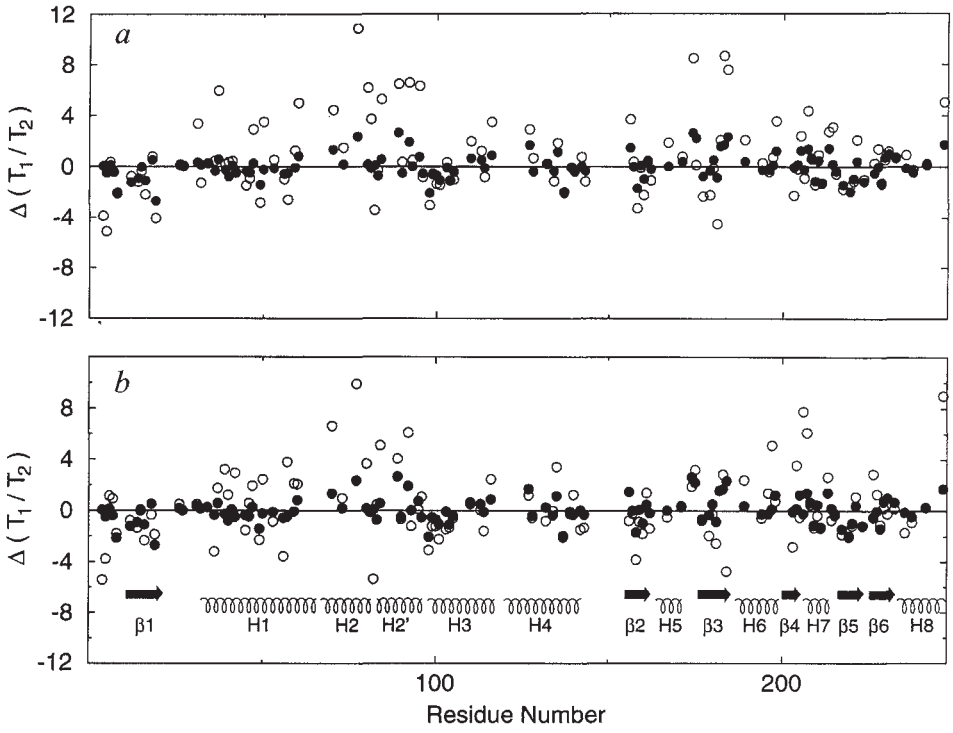

Fig. 3 Plots showing the difference, $\Delta(T_1/T_2)$, between calculated ^{15}N T_1/T_2 ratios as a function of residue number for the restrained regularized mean structure of EIN obtained from the ensembles calculated with—filled-in circles in (*a*) and (*b*)—and without—open circles in (*a*)—^{15}N T_1/T_2 refinement, and for the X-ray structure—open circles in (*b*). The location of the secondary structure elements is displayed in (*b*).

The r.m.s. difference between observed and calculated T_1/T_2 ratios as a function of residue number for the $(\overline{SA}_{anis})r$, $(\overline{SA})r$ and X-ray structures is shown in Fig. 3. The largest deviations (≥ 3.0) between calculated and observed T_1/T_2 ratios for both the $(\overline{SA})r$ and X-ray structures predominantly involve residues located in helices H1 and H2/H2' of the α domain, and strands β2, β3 and β5, and helix H6 of the α/β domain. These deviations are not random but systematic. Thus, for example, the calculated T_1/T_2 ratios for residues in helices H2 and H2' are systematically overestimated, while that of Asp 82 located in the kink between helices H2 and H2' is underestimated. In contrast, the deviations between observed and calculated T_1/T_2 ratios in the $(\overline{SA}_{anis})r$ structure are random and much smaller. The systematic deviations between observed and calculated T_1/T_2 ratios for both the $(\overline{SA})r$ and X-ray structures indicate that the relative orientation of the α and α/β domains in the $(\overline{SA})r$ and X-ray structures are not compatible with the relaxation data. Hence, the dependence of the ^{15}N T_1/T_2 data on rotational diffusion anisotropy permit one to obtain definitive information on the relative orientations of the α and αβ domains in solution and clearly show that this orientation is different in the solution and crystal states.

The difference in the relative orientations of the α and αβ domains between the various structures is best described in terms of the average angular difference between equivalent helices of the α domain when best-fitting the structures to the backbone of the α/β domain (Fig. 1). This angular difference is 5–7° between the $(\overline{SA}_{anis})r$ and $(\overline{SA})r$ structures and between the $(\overline{SA})r$ and X-ray structures, and ~10° between the $(\overline{SA}_{anis})r$ and X-ray structures. It is interesting to note that of the 38 interdomain NOEs, there are no violations in the $(\overline{SA}_{anis})r$ structure, one violation of 0.22 Å in the $(\overline{SA})r$ structure between Arg 136Hε and Ser 166Hβ, and two violations of 0.16 and 0.47 Å between Arg 136Hε and Ser 166Hβ and between Phe 65Hδ and Met 193Hα, respectively, in the X-ray structure. In addition, the X-ray structure predicts two short (<3.5 Å) interdomain interproton distance contacts (Leu 173Hδ–Thr 64Hβ and Ala

Table 2 Backbone (N, Cα, C, O) atomic rms differences[1]

	Backbone atomic rms differences (Å)				
	best-fitted to residues 2–246	best-fitted to αβ		best-fitted to α	
		αβ	α	α	αβ
***a*, Coordinate precision of NMR structures**					
$\langle SA_{anis}\rangle$ *vs* $\overline{SA}_{anis}$	0.80 ± 0.13	0.54 ± 0.11	1.40 ± 0.40	0.52 ± 0.13	1.41 ± 0.50
$\langle SA\rangle$ *vs* $\overline{SA}$	0.94 ± 0.14	0.52 ± 0.16	1.94 ± 0.57	0.55 ± 0.11	2.12 ± 0.74
***b*, Mean coordinate displacements**					
$(\overline{SA}_{anis})r$ *vs* $(\overline{SA})r$	0.77	0.36	2.56	0.40	1.55
$(\overline{SA}_{anis})r$ *vs* X-ray	1.75	1.20	3.17	0.95	2.36
$(\overline{SA})r$ *vs* X-ray	1.53	1.19	2.09	0.92	2.46

[1]The notation of the structures is given in footnote a to Table 1. The α/β domain comprises residues 2–20 and 148–230; the α domain comprises residues 33–143. The X-ray structure is taken from ref. 16.

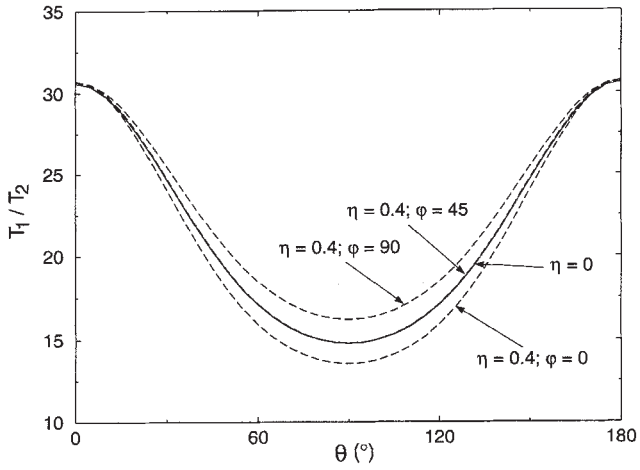

Fig. 4 Effect of rhombicity of the diffusion tensor on the predicted ^{15}N T_1/T_2 ratio. The solid line corresponds to the axially symmetric case, with $2D_{zz}/(D_{xx}+D_{yy}) = 2$. The dashed lines correspond to a fully asymmetric diffusion tensor with $2D_{zz}/(D_{xx}+D_{yy}) = 2$ and $\eta = {}^3/_2(D_{yy}-D_{xx})/[D_{zz}-(D_{yy}+D_{xx})/2] = 0.4$, and ϕ angles of 0°, 45° and 90°. Note that for the case where $\phi = 45° + n \times 90°$ (where n is an integer), the T_1/T_2 ratio becomes virtually indistinguishable from the axially symmetric case. The effective correlation time is 13.1 ns.

169Hα–Ala 61Hβ) which are not observed experimentally in the NOE spectra and have distances greater than 4.7 Å in the NMR structures. Of the 86 NOEs between the linkers and the two domains, there are four violations in the 0.12–0.23 Å range for the $(\overline{SA}_{anis})r$ structure, three in the 0.15–0.23 Å for the $(\overline{SA})r$ structure, and seven in the 0.17–0.91 Å range for the X-ray structure. It is important to note that the relative orientation of the α and αβ domains is not determined by residues with outlying T_1/T_2 ratios; excluding T_1/T_2 restraints for the 18 residues with the largest difference (≥5.0) between predicted and observed T_1/T_2 ratios did not affect the relative orientations of the two domains and resulted in an overall (residues 2–246) backbone atomic r.m.s. shift of only 0.3 Å. Thus, it is the entire ensemble of T_1/T_2 ratios that contributes to the relative domain orientation; outlying T_1/T_2 ratios primarily affect the local backbone torsion angles.

Further tests

To further test the restraining power of the ^{15}N T_1/T_2 restraints, we carried out a series of calculations in which the 38 interdomain interproton distance restraints were removed. Once again, the structures of the individual domains were unaffected by the presence or absence of the relaxation anisotropy restraints. Since the ^{15}N T_1/T_2 restraints for axially symmetric diffusion do not provide any angular information relative to the axis orthogonal to the cylinder axis of the diffusion tensor (that is, twist), they are are not sufficient in their own right to uniquely define the relative orientations of the α and α/β domains. Nevertheless, since the ^{15}N T_1/T_2 restraints define the tilt angle between the two domains, the accuracy (relative to both the SA and X-ray structures) in the orientation of the α domain upon best-fitting the coordinates of the α/β domain is significantly increased upon ^{15}N T_1/T_2 refinement (from ~6 Å to ~4 Å), and the overall accuracy of the structure (that is, obtained by best-fitting residues 2–246) is similarly increased from ~3 Å to ~2 Å.

Effect of rhombicity

In the case of EIN, the diffusion tensor was axially symmetric (that is, $D_{xx} = D_{yy}$). The general, fully asymmetric case, where $D_{xx} \neq D_{yy}$, can be treated in a fully analogous manner. The ^{15}N T_1/T_2 ratio then depends not only on the angle θ between the z axis of the diffusion tensor and the N–H vector orientation, but also on the angle φ which describes the position of the projection of the N–H vector on the x–y plane, relative to the x axis[12–14]. The rhombicity factor, η, is defined as $^3/_2(D_{yy}-D_{xx})/[D_{zz}-0.5(D_{yy}+D_{xx})]$. In practice, for most proteins with large diffusion anisotropy $[2D_{zz}/(D_{xx}+D_{yy}) \geq \sim 1.5]$, η is found to be smaller than 0.4. Even at the high end of this range (η = 0.4) the dependence of the T_1/T_2 ratio on φ is relatively weak (Fig. 4), introducing changes in the predicted T_1/T_2 ratio that are of a magnitude comparable to the uncertainty in the measurements.

Although the effect of rhombicity of the diffusion tensor on the T_1/T_2 ratio is relatively small, including its effect in the structure refinement procedure does not pose any fundamental problem. In this case, the floating diatomic molecule, used above to describe the orientation of the diffusion tensor in the structure calculations for the axially symmetric case, is replaced by a triatomic molecule, ABC, where the AB and BC axes correspond to the z and x axes of the diffusion tensor respectively. Calculation of E_{anis} (Eq. 2) is fully analogous to the axially symmetric case, but uses the full, five-term expression for the spectral density[12]. A set of structure calculations, carried out for a small number of η values (typically 0, 0.2 and 0.4) then indicates whether inclusion of rhombicity leads to better agreement with the experimental T_1/T_2 data. As pointed out above, however, the T_1/T_2 ratio is only a weak function of η and the exact value of η is often poorly defined by the NMR data.

Concluding remarks

In conclusion, we have shown that the dependence of heteronuclear relaxation times on rotational diffusion anisotropy can be used to obtain structural restraints for simulated annealing refinement that define long range order in a simple and straightforward manner. This approach will be particularly useful for multidomain and modular proteins where the orientation of the domains relative to each other is fixed but the number of short interproton distance contacts is too small to permit the orientation of the domains to be defined from the NOE data alone. Examples that immediately come to mind are cell adhesion proteins that contain modules from the immunoglobulin, fibronectin or cadherin superfamilies[3]. The method should also prove to be very powerful for nucleic acids where NOE contacts in the absence of tertiary structure are limited to adjacent basepairs, and even for RNA molecules with tertiary structure, contacts between nucleotides far apart in the sequence are very limited due to the low density of protons. Finally, it should be pointed out that this methodology combined with any method that can make use of the angular dependence of residual dipolar couplings resulting from the partial alignment of a protein along another axis[18,21] (for example, by the use of magnetic susceptibility, electric field or optical anisotropy; unpublished data) could potentially be used to determine a protein fold in the absence of NOE data.

Acknowledgements

We thank A. Szabo for many stimulating discussions. The coordinates and experimental restraints for the structures refined against the ^{15}N relaxation data have been deposited in the Brookhaven Protein Data Bank (2E2A, 2E2B and R2EZAMR). This work was supported in part by the AIDS Targeted Antiviral Program of the Office of the Director of the National Institutes of Health (to G.M.C., A.M.G. and A.B.).

1. Wüthrich, K. *NMR of Proteins.* (Wiley, New York, 1986).
2. Clore, G.M. & Gronenborn, A.M. Determination of three-dimensional structures of proteins and nucleic acids in solution by nuclear magnetic resonance spectroscopy. CRC *Crit. Rev. Biochem. Mol. Biol.* **24**, 479–564 (1989).
3. Bork, K., Downing, A.K., Kieffer, B. & Campbell, I.D. Structure and distribution of modules in extracellular proteins. *Q. Rev. Biophys.* **29**, 119–167 (1996).
4. Allerhand, A. *et al.* Conformation and segmental motion of native and denatured ribonuclease A in solution: application of natural abundance carbon-13 partially relaxed Fourier transform nuclear magnetic resonance. *J. Am. Chem. Soc.* **93**, 544–546 (1971).
5. Lipari, G. & Szabo, A. (1982) Model-free approach to the interpretation of nuclear magnetic resonance relaxation in macromolecules I: theory and range of validity. *J. Am. Chem. Soc.* **104**, 4546–4559.
6. Kay, L.E., Torchia, D.A. & Bax, A. Backbone dynamics of proteins as studied by ^{15}N inverse detected heteronuclear NMR spectroscopy: application to *Staphylococcal* nuclease. *Biochemistry* **28**, 8972–8979 (1989).
7. Clore, G.M., Driscoll, P.C., Wingfield, P.T. & Gronenborn, A.M. Analysis of the backbone dynamics of interleukin-1β using two-dimensional inverse detected 1H-15N NMR spectroscopy. *Biochemistry* **29**, 7387–7401 (1990).
8. Torchia, D.A., Nicholson, L.K., Cole, H.B.R. & Kay, L.E. Heteronuclear NMR studies of the molecular dynamics of staphylococcal nuclease. In *NMR of Proteins* (eds Clore, G.M. & Gronenborn, A.M.)190–219 (MacMillan Press, London, 1993).
9. Wagner, G., Hyberts, S. & Peng, J.W. Study of protein dynamics by NMR. In NMR of Proteins (eds., Clore, G.M. & Gronenborn, A.M.) 220–257 (MacMillan Press, London; 1993).
10. Phan, I.Q.H., Boyd, J. & Campbell, I.D. Dynamic studies of a fibronectin type I module pair at three frequencies: anisotropic modelling and direct determination of conformational exchange. *J. Biomol. NMR* **8**, 369–378 (1996)..
11. Abragam, A. *The Principles of Nuclear Magnetism.* Clarendon Press, Oxford (1961).
12. Woessner, D.E. Nuclear spin relaxation in ellipsoids undergoing rotational Brownian motion. *J. Chem. Phys.* **36**, 647–654 (1962).
13. Tjandra, N., Feller, S.E., Pastor, R.W. & Bax, A. Rotational diffusion anisotropy of human ubiquitin from ^{15}N NMR relaxation. *J. Am. Chem. Soc.* **117**, 12562–12566 (1995).
14. Tjandra, N., Wingfield, P.T., Stahl, S.J. & Bax, A. Anisotropic rotational diffusion of perdeuterated HIV protease from ^{15}N NMR relaxation measurements at two magnetic fields. *J. Biomol. NMR* **8**, 273–284 (1996).
15. Nilges, M., Gronenborn, A.M., Brünger, A.T. & Clore, G.M. Determination of three-dimensional structures of proteins by simulated annealing with interproton distance restraints: application to crambin, potato carboxypeptidase inhibitor and barley serine proteinase inhibitor 2. *Protein Eng.* **2**, 27–38 (1988).
16. Liao, D.-I. *et al.* The first step in sugar transport: crystal structure of the amino-terminal domain of enzyme I of the *E. coli* PEP:sugar phosphotransferase system and a model of the phosphotransfer complex with HPr. *Structure* **4**, 861–872 (1996).
17. Garrett, D.S. *et al.* Solution structure of the 30 kDa N-terminal domain of enzyme I of the *Escherichia coli* phosphoenolpyruvate:sugar phosphotransferase system by multidimensional NMR. *Biochemistry* **36**, 2517–2530 (1997).
18. Tjandra, N., Grzesiek, S. & Bax, A. Magnetic field dependence of nitrogen-proton J splittings in ^{15}N-enriched human ubiquitin resulting from relaxation interference and residual dipolar coupling. *J. Am. Chem. Soc.* **118**, 6264–6272 (1996).
19. MacArthur, M. W. & Thornton, J. M. Deviations from planarity of the peptide bond in peptides and proteins. *J. Mol. Biol.* **264**, 1180–1195 (1996).
20. Brüschweller, R., Liao, X. & Wright, P.E. Long-range motional restrictions in a multidomain zinc-finger protein from anisotropic tumbling. *Science* **268**, 886–889 (1995).
21. Tolman, J.R., Flanagan, J.M., Kennedy, M.A. & Prestegard, J.H. Nuclear magnetic dipole interactions in field-oriented proteins: information for structure determination in solution. *Proc. Natl. Acad. Sci. USA* **92**, 9279–9283 (1995).
22. Koradi, R., Billeter, M. & Wüthrich, K. MOLMOL: a program for display and analysis of macromolecular structures. *J. Mol. Graphics* **14**, 52–55 (1996).
23. Brünger, A.T. *XPLOR Manual Version 3.1* (New Haven, Connecticut: Yale University, 1993).
24. Garrett, D.S., Kuszewski, J., Hancock, T.J., Lodi, P.J., Vuister, G.W., Gronenborn, A.M. & Clore, G.M. The impact of direct refinement against three-bond HN-CαH coupling constants on protein structure determination by NMR. *J. Magn. Reson. Series B* **104**, 99103 (1994).
25. Kuszewski, J., Qin, J., Gronenborn, A.M. & Clore, G.M. The impact of direct refinement against $^{13}C\alpha$ and $^{13}C\beta$ chemical shifts on protein structure determination by NMR. *J. Magn. Reson. Series B* **106**, 92–96 (1995).
26. Kay, L.E., Nicholson, L.K., Delaglio, F., Bax, A. & Torchia, D.A. The effects of cross-correlation between dipolar and chemical shift anisotropy relaxation mechanisms on the measurement of heteronuclear T_1 and T_2 values in proteins: pulse sequences for the removal of such effects. *J. Magn. Reson.* **97**, 359–375 (1992).
27. Peng, J.W., Thanabal, V. & Wagner, G. Improved accuracy of heteronuclear transverse relaxation time measurements in macromolecules: elimination of antiphase contributions. *J. Magn. Reson.* **95**, 421–427 (1991).
28. Grzesiek, S. & Bax, A. The importance of not saturating H_2O in protein NMR: application to sensitivity enhancement and NOE measurements. *J. Am. Chem. Soc.* **115**, 12593–12594 (1993).
29. Brooks, B.R., Bruccoleri, R.E., Olafson, B.D., States, D.J., Swaminathan, S. & Karplus, M. CHARMM: a program for macromolecular energy minimization and dynamics calculations. *J. Comput. Chem.* **4**, 187–217 (1983).
30. Laskowski, R.A., MacArthur, M.W., Moss, D.S. & Thornton, J.M. PROCHECK: a program to check the stereochemical quality of protein structures. *J. Appl. Crystallogr.* **26**, 283–291 (1993).